

Role of interband and photoinduced absorption in the nonlinear refraction and absorption of resonantly excited PbS quantum dots around 1550 nm

Abdoulghafar Omari,^{1,2,*} Iwan Moreels,^{1,2} Francesco Masia,^{3,4} Wolfgang Langbein,³ Paola Borri,⁴ Dries Van Thourhout,^{2,5} Pascal Kockaert,⁶ and Zeger Hens^{1,2,†}

¹Physics and Chemistry of Nanostructures, Ghent University, BE-9000 Ghent, Belgium

²Center for Nano and Biophotonics (NB Photonics), Ghent University, BE-9000 Ghent, Belgium

³Cardiff University School of Physics and Astronomy, The Parade, Cardiff CF24 3AA, United Kingdom

⁴Cardiff University School of Biosciences, Museum Avenue, Cardiff CF10 3AX, United Kingdom

⁵Department of Information Technology, Ghent University-IMEC, BE-9000 Ghent, Belgium

⁶OPERA-Photonics CP 194/5, Université Libre de Bruxelles (U.L.B.), BE-1050 Brussels, Belgium

(Received 5 October 2011; published 23 March 2012)

The nonlinear refractive index n_2 and absorption coefficient β of PbS quantum dots (Qdots) is determined around 1550 nm with the Z -scan technique, using a picosecond pulsed laser. We find that n_2 is wavelength tunable and follows the PbS absorbance spectrum. At fixed wavelength, n_2 is constant in the optical intensity range used (1–25 MW/cm²), indicative of a third order nonlinear effect. The figure of merit is larger than 1 in the quoted intensity range, demonstrating that PbS Qdots are efficient nonlinear materials at telecom wavelengths. It is argued that the creation of excitons and the resulting photoinduced absorption in the PbS Qdots lie at the origin of the observed n_2 and β . Analyzing the measured intensity dependence of the absorption at the first energy transition using a rate-equation model with a full bleaching at 4 excitons per Qdot, we find that photoinduced absorption inhibits the full bleaching of the Qdot first energy transition. Femtosecond four-wave mixing (FWM) experiments at low intensities show that the dynamics of the nonlinear optical response shows a nanosecond decay, which is attributed to exciton thermalization, while at higher excitation intensities an additional ~ 100 ps component appears, which reflects carrier-carrier assisted processes. The analysis of the phase of the FWM signal shows that at high excitation the signal is dominated by photoinduced absorption once charge separation occurs. Considering the facile (wet) processing of colloidal Qdots, these results demonstrate the potential of PbS Qdots for low-cost photonic devices.

DOI: [10.1103/PhysRevB.85.115318](https://doi.org/10.1103/PhysRevB.85.115318)

PACS number(s): 78.67.Bf, 78.47.nj, 78.47.J–, 42.65.Hw

I. INTRODUCTION

Materials with a large nonlinear third-order susceptibility $\chi^{(3)}$ are needed in a wide range of photonic applications. Materials with a large real part of $\chi^{(3)}$ or equivalently a large nonlinear refractive index n_2 are suitable for optical switching, spectral filtering,^{1,2} holography gratings,³ and phase modulated photonic applications. Materials with a large imaginary part of $\chi^{(3)}$ or nonlinear absorption coefficient β are used in many applications including fluorescence imaging, optical data storage, microfabrication,^{4–6} and saturable absorbers for optical limiting and mode locked lasers and generally in photonic applications where an amplitude modulation is required. Table I lists values of n_2 , β , and the corresponding figure of merit FOM ($n_2/\lambda\beta$), measured around $\lambda = 1.55 \mu\text{m}$, for typical bulk semiconductors,^{7,8} chalcogenide glasses,^{9–11} and nonlinear polymers.^{12,13} Materials such as GaAs, Si, or silica have a poor FOM around the telecom wavelengths (1.55 μm), making them unsuited for integrated nonlinear photonic devices. A way to enhance their performance is functionalization by the overgrowth of high FOM materials, such as AlGaAs or chalcogenide glasses. However, due to the high cost of vacuum-based deposition routes, these materials are less favorable for large-area processing.¹⁴ This drawback can be overcome by the use of solution-deposited materials with a large FOM. For instance, all-optical signal processing has been recently demonstrated by functionalizing Si slotted waveguides with 2-[4-(dimethylamino)phenyl]-3-([4(dimethylamino)phenyl]-

ethynyl)buta-1,3-diene-1,1,4,4-tetracarbonitrile (DDMEBT) polymers.¹⁵

Colloidal semiconductor nanoparticles or Qdots are an appealing alternative class of materials, due to the combination of size-tunable optical properties and a suitability for wet processing. They possess a high photoluminescence efficiency, making them potential light sources in LEDs^{16,17} and lasers^{18–20} and they have a high and tunable absorption cross section, enabling the fabrication of efficient near infrared (NIR) photodetectors.^{21,22} Furthermore, it has been shown that PbSe Qdots have a high and tunable n_2 upon resonant excitation around 1.55 μm ,²³ and the use of PbS Qdot doped glasses as saturable absorbers for passive mode locking in Yb:KYW and Cr⁴⁺:YAG lasers has been demonstrated.^{24,25} Recently, Padilha *et al.*²⁶ and Nootz *et al.*²⁷ have investigated the absorption cross sections for nonresonant two photon absorption (TPA) of PbS and PbSe QDs. Other authors have studied the nonlinear optical properties of PbS Qdots at wavelengths ranging from 0.5 μm to 1.1 μm .^{28–33} Yoshino *et al.*^{34,35} investigated the nonlinear optical properties for PbS Qdot suspensions with a first exciton peak at 1.33 μm excited in the wavelength range 1.1–1.6 μm . In the same wavelength range, Brzozowski *et al.* reported values for FOM up to 0.3 for PbS Qdot suspensions with a first exciton peak at 1.39 μm .³⁶ Savitski *et al.*³⁷ have studied the nonlinear absorption of PbS Qdots doped glasses in the wavelength range 1.06–1.54 μm .

In spite of this extensive research, however, no studies report on n_2 , β , and the resulting FOM for PbS Qdots resonantly excited around 1.55 μm . Here, we study nonlinear

TABLE I. The nonlinear refractive index n_2 , the nonlinear absorption coefficient β , and figure of merit FOM for typical materials, measured around $\lambda = 1.55 \mu\text{m}$.^{7-13,38}

Material	n_2 $10^{-13} \text{ cm}^2/\text{W}$	β cm/GW	FOM $n_2/(\lambda\beta)$
Fused Silica	0.0027
Semiconductors			
Si	0.45	0.79	0.37
GaAs	1.59	10.2	0.1
AlGaAs	1.75	0.35	3.2
Chalcogenide glasses			
Ge ₂₅ As ₁₀ Se ₆₅	0.6	0.4	1.0
Ge ₃₃ As ₁₂ Se ₅₅	1.5	0.4	2.4
As ₄ S ₃ Se ₃	1.2	0.15	5
As ₄₀ S ₆₀	0.6	<0.03	>12
Polymers			
DDEMBT	1.7	...	2.19

refraction and absorbance of PbS Qdots using picosecond pulsed excitation between 1535 and 1565 nm. Using the Z-scan technique in combination with chopped illumination, we find that a dispersion of PbS Qdots shows strong nonlinear refraction due to electronic effects. Although related to absorption saturation, we argue that photoinduced intraband absorption also contributes to n_2 . Next, using pump-probe four wave mixing (FWM), we determine the time response of the optical nonlinearity. We demonstrate that it contains a nanosecond component at low excitation intensities. With increasing light intensity, the FWM decay contains an additional ~ 100 ps component, which we attribute to the presence of carrier-carrier mediated scattering processes, next to a dip prior to the rise of the FWM signal. This unexpected dip may reflect the destructive interference between two FWM signals, the bleaching of the QD absorption (with a typical time constant set by the exciton lifetime) and photoinduced absorption.

II. EXPERIMENTAL

A. Setup and beam characterization

1. Z-scan technique

For the Z-scan measurements,³⁹ we used a setup as shown in Fig. 1(a). In brief, a pulsed, Gaussian laser beam with a repetition rate ν is guided toward a lens L1 (using for instance a mirror M1), which creates a focused Gaussian beam. To correct for possible fluctuations of the laser intensity during the measurement, a small fraction is reflected at beam splitter BS1 and monitored at detector D1. The linear stage LS translates the sample S along the z axis through the focus of the Gaussian beam. After passing through the sample, a fraction of the total beam intensity (TBI) is reflected at beam splitter BS2 and measured with detector D2, while the on-axis intensity (OAI) is measured in the far field of the laser beam with a small aperture A and detector D3. The input intensity is set using a variable neutral density filter NDF. The illumination of the sample can be chopped using an electronic shutter ESH.

The Gaussian spatial profile induces a lens in a nonlinear sample, creating an extra (de)focusing of the beam [see

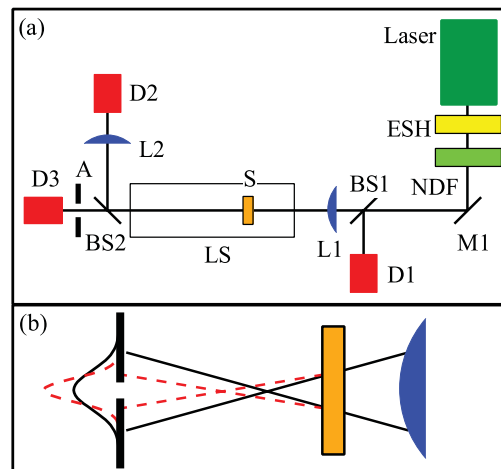


FIG. 1. (Color online) (a) Schematic representation of the Z-scan setup. (b) Far away from the laser beam focal point, the optical intensity is too low to induce nonlinear effects (full lines). Near the focus, at prefocal positions, the sample acts as a thin lens, inducing an extra beam divergence in the case of a negative n_2 (dashed lines). This leads to an increased on-axis intensity.

Fig. 1(b)], enabling the determination of n_2 . In our experiments, we use a 10 MHz pulsed laser with a pulse duration of $\tau_p \approx 2.5$ ps. τ_p is determined with an optical autocorrelator; the pulses have a Gaussian temporal profile. The beam is spatially characterized by two parameters: the beam waist w_0 (beam radius at the focus) and the Rayleigh length z_R . At a given wavelength λ , both are related through

$$z_R = \frac{\pi w_0^2}{\lambda M^2}, \quad (1)$$

where M^2 denotes the beam quality factor, which equals one for a Gaussian (diffraction limited) beam. We determine w_0 and z_R with a beam profiler at $\lambda = 1550$ nm. The resulting $w_0 = 47 \mu\text{m}$ and $z_R = 3.9$ mm yield $M^2 = 1.17$, confirming that the beam has a Gaussian spatial profile.

Another important characteristic is the on-axis power density at the focus I_0 (referred to as the optical intensity from here on). I_0 equals the maximal power density achieved during a laser pulse. We calculate I_0 from the measured average laser power P :

$$I_0 = \frac{2}{\sqrt{\pi}} \frac{P}{\nu \tau_p \pi w_0^2}. \quad (2)$$

B. Derivation of n_2 and β from the Z-scan traces

A calculation of n_2 and β starts from the differential equations that describe the attenuation and phase change of an electric field as it passes through a nonlinear sample with length L .³⁹ We assume that the sample nonlinearity is limited to the third order ($n = n_0 + n_2 I_0$, $\alpha = \alpha_0 + \beta I_0$) and that the sample length L is much smaller than the Rayleigh length ($L \ll z_R$, thin sample approximation). Using the following substitutions: $q = \beta I_0 L_{\text{eff}}$ (L_{eff} : effective sample length)³⁹ and $x = z/z_R$, this yields for the normalized TBI trace:

$$T_{\text{TBI}}(x) = \frac{(1+x^2)}{q} \ln \left(1 + \frac{q}{1+x^2} \right). \quad (3)$$

Equation (3) enables us to determine q , and therefore β , from a fit to the experimental TBI trace.

The normalized OAI is derived in a similar way:

$$T_{\text{OAI}}(x) = (1 + x^2) \left| \sum_{m=0}^{\infty} \frac{(i \Delta\phi_0)^m (2m + 1 + ix)}{m!(1 + x^2)^m [(2m + 1)^2 + x^2]} \right|^2. \quad (4)$$

For practical calculations, we limit ourselves to an approximation up to the third order in the nonlinear phase shift $\Delta\phi_0$.²³

$$\begin{aligned} T_{\text{OAI}}(x) = & 1 + \frac{4x}{(x^2 + 1)(x^2 + 9)} \Delta\phi_0 \\ & + \frac{4(3x^2 - 5)}{(x^2 + 1)^2(x^2 + 9)(x^2 + 25)} \Delta\phi_0^2 \\ & + \frac{32x(x^2 - 11)}{(x^2 + 1)^3(x^2 + 9)(x^2 + 25)(x^2 + 49)} \Delta\phi_0^3. \end{aligned} \quad (5)$$

We estimate that the first-order approximation (the one most often used in literature) is valid up to $\Delta\phi_0 \approx 0.2$, the second order up to $\Delta\phi_0 \approx 1$, and the third order up to $\Delta\phi_0 \approx 1.75$. The validity is within an error of less than 3.5% in determining the OAI transmission and predicting the focal position ($x = 0$). By fitting the OAI trace to Eq. (5), we can determine $\Delta\phi_0$ and thus n_2 according to

$$\Delta\phi_0 = \frac{2\pi n_2 I_0 L_{\text{eff}}}{\lambda}. \quad (6)$$

C. Thermal effects

When performing Z-scan measurements using a nontransparent material (as is the case here, as we study the *resonant* nonlinearities of PbS Qdots around the band gap), the absorbed energy can be converted to heat. The corresponding temperature increase of the sample may also lead to a change in refractive index, due to the thermo-optical coefficient dn/dT . In the center of the laser beam, the higher optical intensity leads to a higher increase in temperature than at the edges of the laser beam. Hence, taking heat diffusion throughout the material into account, a steady-state spatial temperature profile will develop at $t \gg t_c$, with $t_c = w_0^2/(4D)$ the characteristic profile buildup time. D denotes the thermal diffusion coefficient of the medium. If dn/dT differs from zero, the refractive index will follow this temperature profile, leading to a thermal lensing effect⁴⁰ (similar to the electronic lensing effect described above).

The resulting OAI trace will also show an antiresonance. Taking only linear absorption into account, i.e., neglecting nonlinear processes such as TPA, the *thermal* OAI can be described by⁴⁰

$$T_{\text{OAI,th}}(x) = 1 + \theta \arctan\left(\frac{2x}{x^2 + 3}\right). \quad (7)$$

The equation is valid for a small thermal lens strength θ :

$$\theta = \frac{\alpha_0 L P}{\lambda \kappa} \frac{dn}{dT}. \quad (8)$$

As expected, θ depends only on the average power and is inversely proportional to the thermal conductivity κ , as a larger κ leads to a more rapid heat dissipation.

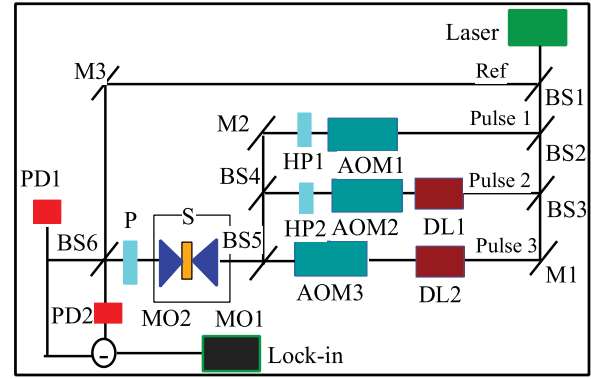


FIG. 2. (Color online) Schematic representation of the FWM setup.

1. Four wave mixing (FWM)

The Z-scan measurement as described above yields the absolute values of the nonlinear refractive index and absorption coefficient, but it provides no information on the dynamics of the optical nonlinearity. To investigate this, we measure the time-resolved response of the optical nonlinearities using a FWM setup (see Fig. 2).⁴¹ A Ti:Sapphire laser pumps an optical parametric oscillator (APE OPO) that provides pulses of 150 fs duration around $1.47 \mu\text{m}$ with 76 MHz repetition rate. The laser beam is split up into four components denoted as reference, pulse 1, pulse 2, and pulse 3 (R, P_1, P_2, P_3). The frequencies of the pulses are upshifted using acousto-optical modulators to 79, 80, and 80.6 MHz for P_1, P_2 , and P_3 , respectively.⁴² P_1 and P_2 as well as P_2 and P_3 are mutually time delayed by τ_{12} and τ_{23} by means of delay stages (DL) with a temporal resolution of 20 fs. All exciting pulses are combined through BS5 and sent through the sample S (thin film) using an oil-immersion microscope objective MO1 with a numerical aperture of $\text{NA} = 1.25$.

P_1 creates a coherent polarization in resonance with the band-gap transition of the sample. P_2 arrives in time-overlap ($\tau_{12} = 0$) to ensure that the coherent polarization is not lost and interferes maximally with P_1 . This induces a carrier density modulation over the pulse repetitions, which in turn modulates the absorption and hence the transmission of P_3 . The measured FWM field is E_{FWM} is proportional to

$$E_{\text{FWM}} \propto \chi^{(3)} E_1 E_2^* E_3 \quad (9)$$

with the third-order susceptibility $\chi^{(3)}$. $E_{1,2,3}$ are the optical electric fields associated with $P_{1,2,3}$ in the sample, having an amplitude proportional to $\sqrt{I_{1,2,3}}$. The FWM field is measured through its interference with the reference field, which is in time overlap with P_3 . The dynamics of the modulated carrier density can be obtained by measuring E_{FWM} as a function of the delay τ_{23} . $P_{1,2}$ were chosen linearly co-polarized by half-wave plates (HP). Both were cross polarized to P_3 and R to reduce the background from the balanced photodetectors (BPD) and maximize the heterodyne detection of the FWM signal.

D. Sample preparation and nonlinear measurements

All following measurements (Z-scan and FWM) were performed at room temperature. For our study of the n_2 of

TABLE II. Summary of the different samples used for the Z-scan and FWM experiments. λ_0 denotes the spectral position of the first absorption peak and c_0 the sample concentration.

Sample	Size (nm)	λ_0 (nm)	c_0 (μM)
A	3.8	1123	4.95
B	5.2	1408	5.45
C	5.5	1492	6.34
D	5.9	1539	4.91
E	6.1	1574	4.63
F	6.4	1620	4.76
G-I	5.9	1539	0.48,1.37,2.89
J,K	5.9	1539	6.06,9.78
L	5.6	1506	Thin film

PbS Qdots, we prepared 12 Qdot samples. All the samples have a size dispersion of $\approx 5\%$. The sample optical properties are very stable in time.⁴³ Their properties are summarized in Table II. The concentrations of all samples are optimized to obtain a clearly measurable $\Delta\phi_0$, while still keeping its value low enough for the fit [see Eq. (5)] to apply ($\Delta\phi_0 < 1.75$). We use a $L = 1$ mm optical cell for the Z-scan measurements, satisfying $L \ll z_R$. The Qdots are suspended in C_2Cl_4 , a transparent solvent in the NIR spectral range. Z-scan traces recorded for C_2Cl_4 are featureless both for the TBI and OAI, revealing a negligible n_2 and β of the solvent. To determine the spectral dependence of n_2 for our Qdot suspensions, Z-scan traces are measured between 1535 and 1565 nm. The intensity dependence of n_2 is measured between 1 and 25 MW/cm^2 , at $\lambda = 1550$ nm.

For sample D, E, and F, we determine the intensity dependence of the nonlinear absorption coefficient β . Samples D, E, G–K are used to explore the nonlinear absorption further by positioning the sample at the focus and collecting the sample transmittance T as a function of I_0 . I_0 is varied between 0.5 and 25 MW/cm^2 , around $\lambda = 1550$ nm. From T , the intensity-dependent absorption coefficient is calculated: $\alpha = -\ln(T)$. We use samples D, G–K to determine the concentration dependence of n_2 , β , and α .

For the FWM measurements, we prepared sample L using a 20- μM solution of PbS Qdots mixed with a solution 10 m% of polystyrene in toluene. The solution is spin coated with a spinning speed of 1000 rpm on a 0.17 mm glass coverslip. The resulting film has a uniform thickness of ≈ 2 μm and macroscopically homogenous concentration of PbS QDs. The sample is then mounted on another coverslip of same thickness by using Meltmount (Cargille Labs) (refractive index 1.54) as mounting medium. For the FWM experiment, the total average intensity used is varied between 0.7 to 89 kW/cm^2 , corresponding to peak intensity from 0.054 to 6.9 GW/cm^2 .

III. RESULTS AND DISCUSSION

A. Excluding thermal effects

Typical OAI and TBI traces for a Qdot suspension are shown in Fig. 3. The OAI shows a strong antiresonance [see Fig. 3(a)], that can only be satisfactorily fitted to a sum of Eqs. (5) and (7) [see Fig. 3(b)]. The TBI features an increase in intensity near the focus indicating a negative β [see Fig. 3(c)].

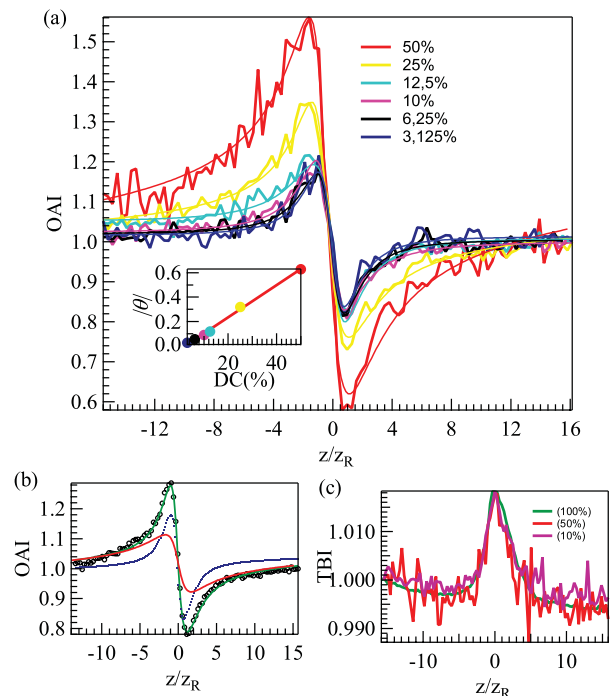


FIG. 3. (Color online) (a) Typical experimental OAI traces, measured on $\lambda = 1550$ nm for sample D as a function of ESH duty cycle. The OAI shows a strong antiresonance. Inset: when reducing the DC, the magnitude of the thermal lens strength decreases. (b) Illustration for the traces fitted (black dots) with a sum of Eq. (5) (blue line) and (7) (red line) for sample D at a DC = 12%. (c) The corresponding measured TBI traces for sample D. The TBI remains constant when changing the duty cycle and yields an increase around the focus indicating a negative β .

Using the ESH, we switch the laser light between *on* for 2 ms and *off* for a time interval variable between 0 and 64 ms, corresponding to a duty cycle (DC) between 100% and 3%, respectively. As shown in Fig. 3(a), we find that reducing DC from 100% to 12.5% leads to a steady decrease of the OAI peak and valley amplitude. Below 12.5%, the OAI trace tends toward a limiting trace when DC is further reduced. In addition, no change in the limiting trace is obtained when reducing the on time to 1 ms keeping the same duty cycle. In Fig. 3(c), one sees that the TBI remains constant when sweeping the DC.

The above observations indicate that at a DC of 12.5% or more, the OAI is composed of an electronic and a thermal component. Using the fit of the OAI to a sum of an electronic and a thermal nonlinearity, we determined dn/dT . Limiting the DC to 12.5% to ensure the low thermal lens strength condition, we obtain a value of $-0.9 \times 10^{-4} \text{ K}^{-1}$, which stays constant in the range 1535–1565 nm. Independent measurements of dn/dT for CCl_4 , CHCl_3 , and CH_2Cl_2 , performed at visible wavelengths, yield values of about $-6 \times 10^{-4} \text{ K}^{-1}$.^{44,45} As we find a number of the same order of magnitude, we conclude that the energy absorbed by the Qdots is, at least, partially converted to heat and transferred to the surrounding C_2Cl_4 medium. Using the material properties of C_2Cl_4 ($D = 7.7 \times 10^{-8} \text{ m}^2/\text{s}$),⁴⁶ we calculate a t_c of 4.7 ms. Hence, a duty cycle of 7.3% or less is needed to prevent the buildup of a stationary thermal lens. In line with these findings, we fix DC at 3.1%

for further measurements. This excludes thermal contributions and allows the determination of n_2 by fitting OAI traces using only the electronic contribution of Eq. (5).

B. Nonlinear refraction (n_2) and absorption (β) for PbS quantum dots

Figure 4(a) shows typical OAI traces obtained for sample K at two different light intensities. As indicated in Fig. 4(b), this results for the PbS Qdot concentrations used (4.5–6.5 μM) in a nonlinear refractive index n_2 of the order of $10^{-11} \text{ cm}^2/\text{W}$, a value independent of I_0 in the intensity range $I_0 = 1\text{--}25 \text{ MW}/\text{cm}^2$ around $\lambda = 1550 \text{ nm}$. By changing the Qdot concentration in solution, we find that n_2 changes proportionally to the Qdot volume fraction f [see Fig. 4(c)]. From the regression curve, we get a concentration independent intrinsic nonlinear refractive index $n_{2,\text{int}} = n_2/f$ of $-1.17 \times 10^{-7} \text{ cm}^2/\text{W}$, a value of the same order of magnitude as the $-6.51 \times 10^{-7} \text{ cm}^2/\text{W}$ measured for PbSe Qdots at $\lambda_0 = 1640 \text{ nm}$.²³ Figure 5 represents the spectral dependence of n_2 for samples A–F, measured between 1535 and 1565 nm and rescaled to a concentration value of 5 μM . As the wavelength range is limited, an alternative representation of n_2 is given, in which the abscissa is the difference between the laser wavelength and the absorption wavelength λ_0 of the Qdots. In agreement with the n_2 spectrum of PbSe Qdots,²³ we find that n_2 is correlated with the absorbance spectrum of the PbS Qdot suspensions.

A suitable parameter to assess the measured values for n_2 is the figure of merit [FOM = $\delta n/(\lambda\alpha)$]. It is a materials property, independent of the Qdot volume fraction and reflects the maximal nonlinear phase shift that can be achieved when light propagates through a sample, before absorption reduces its intensity too much for nonlinear effects to occur. Within the intensity range studied, we find FOMs that are larger than

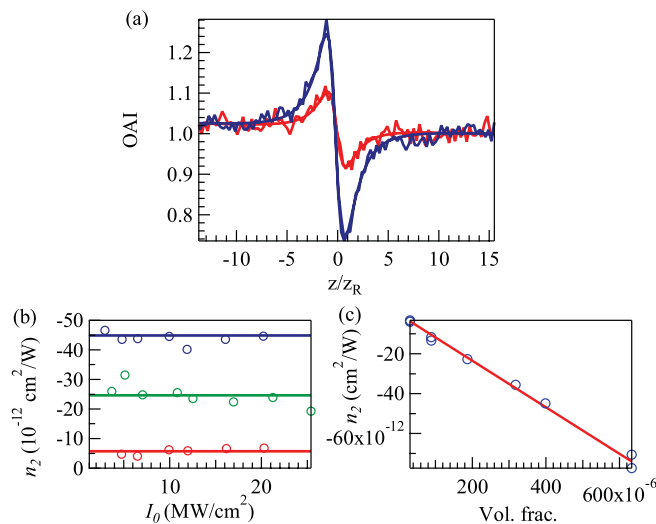


FIG. 4. (Color online) (a) Measured OAI for sample K at intensities of 2.7 and 8.0 MW/cm^2 at a DC = 3.1% fitted with Eq. (5). (b) Dependence of n_2 on I_0 for samples J, E, F (blue, green, and red dots). n_2 remains constant over the entire intensity range. (c) n_2 increases linearly with the Qdot volume fraction measured for samples with first absorption peak at 1539 nm (see Table II).

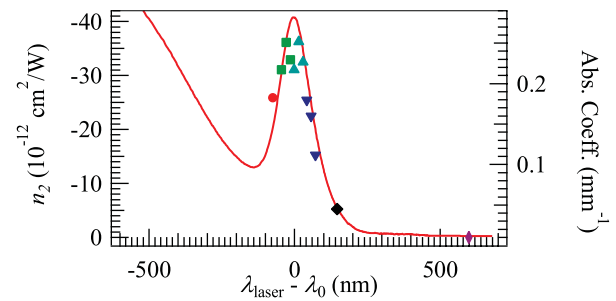


FIG. 5. (Color online) n_2 spectra around 1550 nm. λ_0 denotes the absorption peak of the sample and λ_{laser} is the varying laser wavelength. n_2 is clearly correlated with the Qdot absorption coefficient. The symbols are from right to left: diamond (sample A), square (sample B), downward triangles (sample C), upward triangles (sample D), squares (sample E), and dot (sample F).

one and that increase with increasing light intensity. Since these values are similar to the FOM of AlGaAs⁷ and the chalcogenide glasses^{9–11} (see Table I), PbS Qdots are clearly of interest as nonlinear optical materials.

Figure 6(a) shows the nonlinear absorption coefficient β as determined for three different PbS samples. In line with the TBI trace given in Fig. 3(c), β is negative and is largest for λ_0 closest to the excitation wavelength. Similar to n_2 , the magnitude of β increases with the volume fraction. A linear fit yields an intrinsic nonlinear absorption coefficient $\beta_{\text{int}} = \beta/f$ of $-2.47 \times 10^5 \text{ cm}/\text{GW}$. On the other hand, Fig. 6(a) indicates that the magnitude of β —as determined from a fit of the TBI

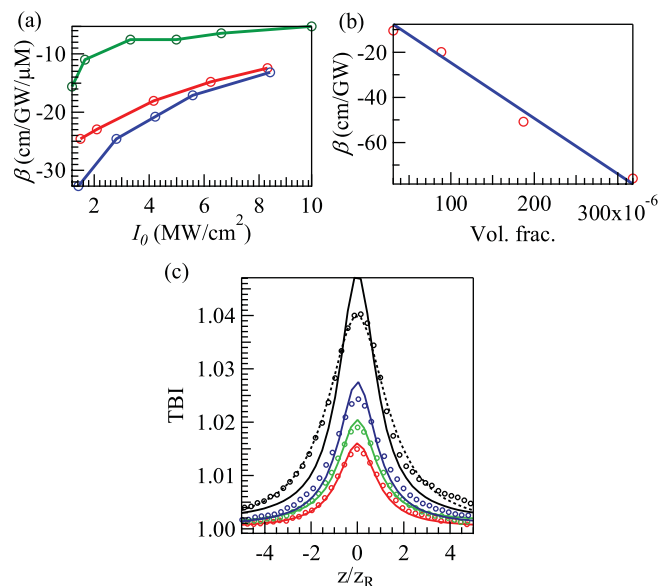


FIG. 6. (Color online) (a) The magnitude of β (normalized to corresponding concentration) decreases with increasing I_0 . Blue, red, and green curves correspond to sample D, E, and F, respectively. (b) β scales linearly with the Qdot volume fractions measured for samples with $\lambda_0 = 1539 \text{ nm}$. (c) TBI traces for sample D at optical intensities of 1.7, 2.5, 3.7, and 8.4 MW/cm^2 fitted with Eq. (3) (full lines). At $I_0 = 8.4 \text{ MW}/\text{cm}^2$, the TBI fits only with Eq. (14) (dotted black line) as it broadens compared with the predicted fit from a true third-order nonlinearity (full black line).

Eq. (3)—decreases with increasing intensity. In addition, the TBI [see Fig. 6(c)] broadens at intensities above 8 MW/cm² and no longer fits to Eq. (3).

C. Intensity dependence of the absorption coefficient (α)

The broadening of the TBI and the decrease of β with increasing I_0 point toward absorption saturation. To investigate this, we have directly measured the absorbance α as a function of the optical intensity I_0 (sample D and E). The Qdots are probed at 1550 nm, on resonance with their band gap transition. Figure 7(a) shows that, at low optical power, the linear absorbance α_0 is recovered. In line with the negative nonlinear absorption coefficient, α decreases with increasing I_0 , which suggests bleaching induced by state filling.

Assuming an eightfold degeneracy of the PbS HOMO and LUMO, one expects that the absorbance of a QD decreases

linearly with the number of excitons γ it contains, to reach zero when $\gamma = 4$.⁴⁷

$$\alpha = \frac{(8 - 2\gamma)}{8} \alpha_0. \quad (10)$$

The expected complete bleaching at $\gamma = 4$ contrasts with conclusions from Refs. 48 and 49, yet forms a relevant starting point to benchmark our results. As a reference, the top axis in Fig. 7(a) gives the average number of photons N_{ex} absorbed per Qdot by a single pulse with an intensity as given by the bottom axis (see Appendix A). At the highest light intensities used, N_{ex} reaches one. Since the exciton lifetime of about 1 μ s exceeds the 100 ns time delay between successive pulses, this indicates that the measured change of the absorbance is not due to a single pulse event, yet results from the buildup of excitons over several pulses. Based on this picture and Eq. (10), we have calculated $\alpha(I_0)$ by using a rate equation model involving band gap absorption and stimulated emission (see Appendix B). For this calculation, we assumed a homogenous linewidth ΔE_{hom} of the Qdot's first exciton transition of 18 meV. This is a 300 K value extrapolated from low-temperature data determined by exciton dephasing in an ensemble of QDs done with photon-echo spectroscopy.⁵⁰ As shown in Fig. 7(a), this results in a theoretical $\alpha(I_0)$ considerably smaller than the measured one. The same conclusion holds if ΔE_{hom} is set equal to the total linewidth of 58.5 meV, a value that follows from the FWHM of the first exciton transition in the Qdot absorption spectrum. In line with our experiment, previous measurements on PbS suspensions^{48,49} did not yield complete absorption bleaching at high excitation intensities.

This indicates that an excited Qdot is a stronger absorber than predicted by Eq. (10). As shown in Fig. 7, a possible origin of this enhanced, photoinduced absorption are intraband transitions that bring the first exciton (labeled as GS in Fig. 7) to an excited single exciton state (ES in Fig. 7). A similar observation was made in lead salt Qdot doped glasses.^{29,37}

If the electrons in the conduction band and the holes in the valence band of excited Qdots can be excited to higher energy conduction band or lower energy valence band states, one expects an additional contribution to α that is proportional to the number of excitons:

$$\alpha = \frac{(8 - 2\gamma)}{8} \alpha_0 + \frac{\gamma}{4} \alpha_{\text{pi}}. \quad (11)$$

Clearly, the occurrence of photoinduced absorption inhibits the bleaching of the Qdot band gap transition when $\gamma = 4$. If we base our calculation of $\alpha(I_0)$ on Eq. (11), a fit with the experimental curve yield $\alpha_{\text{pi}} = 0.4 \alpha_0$. By including photoinduced absorption in the proposed two-level model, the theory fits well with the experimental results.

Figure 7(b) shows that for practical purposes, the experimental $\alpha(I_0)$ can be fitted by extending the expression for the intensity dependence of the absorbance of a two-level system with a nonsaturable absorption coefficient α_{ns} .⁵¹

$$\alpha = \frac{\alpha_0 - \alpha_{\text{ns}}}{1 + I_0/I_{\text{sat}}} + \alpha_{\text{ns}}. \quad (12)$$

This includes a saturation intensity I_{sat} , which corresponds to the value of I_0 where the absorbance is halfway between α_0 and α_{ns} . Typical values for the fitting are $I_{\text{sat}} = 7.2 \text{ MW/cm}^2$

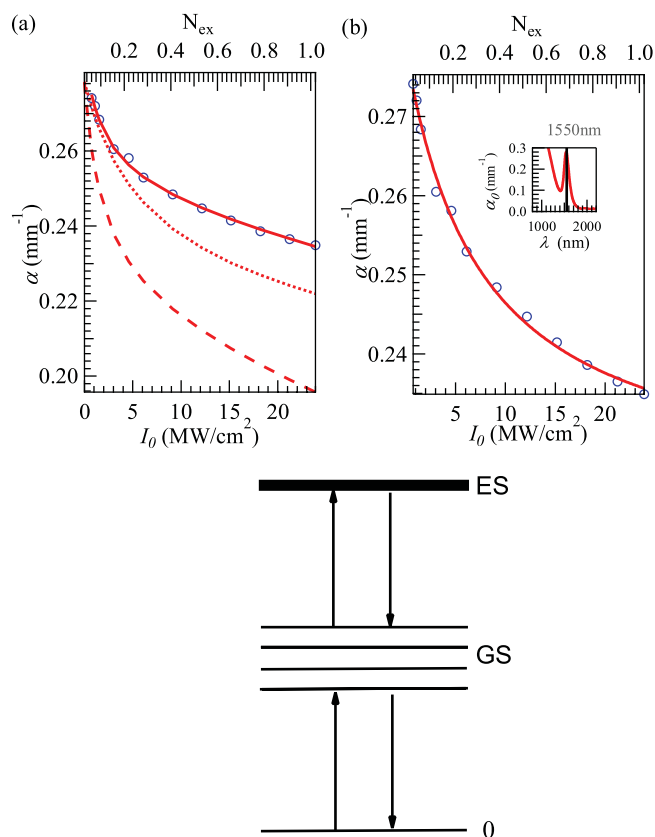


FIG. 7. (Color online) (a) When we exclude the absorption from an exciton ground state (GS) toward an exciton excited state (ES) [see Eq. (10)] the theoretically expected absorption, assuming a Qdot homogeneous linewidth (ΔE_{hom}) of 18 meV (dashed line), is smaller compared with the measured one (blue circles). Neglecting the contribution of the inhomogeneous broadening and assuming the total linewidth is all due to homogeneous broadening ($\Delta E_{\text{hom}} = \Delta E_{\text{total}} = 58$ meV) the corresponding increase in absorption (dotted line) is not sufficient to explain the measurements. If we include the absorption from GS to ES, the measurements fit well with the rate equation model with $\Delta E_{\text{hom}} = 18$ meV. (b) Measured α fitted with expression (12). Inset: absorption spectrum (α_0) of sample D.

and $\alpha_{\text{ns}}/\alpha_0 = 0.8$. By using Eq. (12) to describe $\alpha(I_0)$, we can reinterpret the TBI traces measured in Fig. 6(c). For this, we divide the intensity I_0 in Eq. (12) with a factor $(1 + x^2)$, where $x = \frac{z}{z_R}$, to take into account the Gaussian spatial dependence of the intensity:

$$\alpha(x, I_0) = \frac{\alpha_0 - \alpha_{\text{ns}}}{1 + I_0/[I_{\text{sat}}(1 + x^2)]} + \alpha_{\text{ns}}, \quad (13)$$

$$T_{\text{TBI}} = e^{-\alpha(x, I_0)L}. \quad (14)$$

At low light intensities, Eq. (14) reduces to Eq. (3), which holds for a third-order nonlinearity. With increasing light intensity, however, only (14) fits to the experimental, broadened TBI traces.

D. Dynamics of optical nonlinearities in PbS quantum dots

Since the nonlinear optical properties of PbS Qdots are related to the creation of excitons, one expects that the relaxation and recombination of these excitons determines the dynamics of their optical nonlinearity. We analyzed this nonlinear dynamics using FWM as described in Sec. II C 1. Figure 8(a) represents the FWM amplitude as measured on PbS Qdots (sample L) excited at $\lambda_{\text{ex}} = 1470$ nm as a function of the time delay between P_2 and P_3 . The different traces correspond to different intensities of the P_1 pulse (with P_2 and P_3 having same intensity as P_1) expressed in terms of N_{ex} . N_{ex} has been calculated considering the constructive interference between P_1 and P_2 leading to an effective intensity $4I_1$. The intensity has been tuned such that the FWM experiments correspond to the same range of N_{ex} (0–3) as used in the Z-scan measurements (see Fig. 7 a). Figure 8(a) clearly shows that with increasing excitation intensity, the resolved FWM dynamics has a larger amplitude and a faster decay. Moreover, a dip appears at time overlap.

We have analyzed the FWM dynamics using the following response function:

$$E_{\text{FWM}}(\tau_{23}) = \Theta(\tau_{23})(A_1 e^{-\frac{\tau_{23}}{T_1}} + A_2 e^{-\frac{\tau_{23}}{T_2}}) + A_{\text{os}}. \quad (15)$$

The sum of two exponentials multiplied by a step function $\Theta(\tau_{23})$ represents the response after the excitation. The offset A_{os} is included to account for the accumulation of excitons/charges over successive pulses since the single exciton lifetime of about $1 \mu\text{s}$ ⁴³ strongly exceeds the repetition period of the laser (13 ns). The FWM dynamics is then fitted considering the convolution of the response function with a Gaussian pulse intensity autocorrelation, which transforms an instantaneous contribution into the Gaussian pulse autocorrelation and a step-function into an error function. For the contributions A_1 and A_2 , we find lifetimes in the range 1–4 ns (T_1) and 45–110 ps (T_2). Figure 8(b) shows the amplitude of each contribution normalized to the amplitude $|E_3|$ of the P_3 field as a function of I_1 .

At peak excitation intensities below 0.13 GW/cm^2 ($N_{\text{ex}} < 0.17$) the decay is dominated by the nanosecond component. Similar to what was reported previously on PbS Qdots of smaller size,⁴¹ we attribute this nanosecond dynamics to phonon-assisted single exciton thermalization between the 64 1S-like energy states. This interpretation is confirmed by the linear increase of $A_1/|E_3|$ with the excitation power in the low-intensity regime, which indicates a single exciton process.

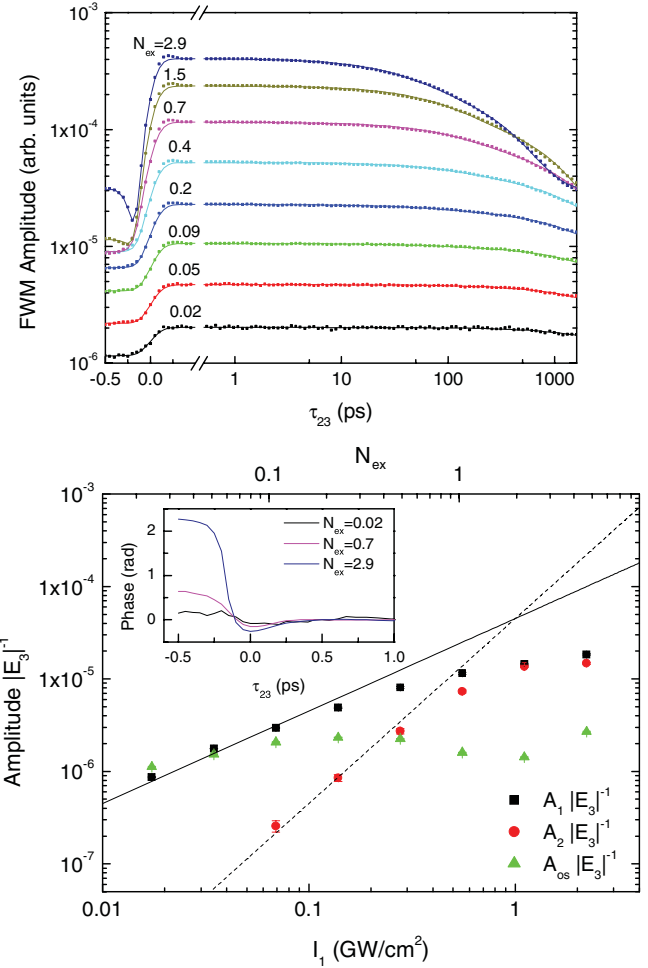


FIG. 8. (Color online) (a) Measured FWM for sample L as a function of the averaged excitations per QD created per pulse, N_{ex} . (b) Amplitude of each recombination mechanism (see text) divided by the P_3 field amplitude as a function of P_1 intensity (I_1). Solid and dashed lines show a linear and quadratic dependencies with the excitation intensity, respectively. In the inset: dynamics of the FWM field phase for different excitation intensities around $\tau_{23} = 0$, relative to the phase at $\tau_{23} = 0.5$ ps.

With increasing optical intensity, the picosecond component becomes more and more important. The time constant T_2 is constant over the intensity range investigated (110 ± 20 ps), apart for the maximum intensity where it drops to 45 ps. $A_2/|E_3|$ follows a quadratic dependence on excitation intensity and eventually saturates at high I_1 . Such dynamics with quadratic intensity dependence could be attributed to Auger-like nonradiative recombination of biexcitons created in a single pulse repetition. However, in smaller PbS dots, where the probability for Auger processes is expected to be larger, we found no evidence of such biexciton recombination.⁴¹ Alternatively, this component can be explained as thermalization of single excitons between the different levels of the ground state mediated by carrier-carrier scattering. Notably, the nanosecond time constant varies from 4.3 ns at 0.02 GW/cm^2 to 0.33 ns at 2.2 GW/cm^2 , with a low-intensity dependence of $I_1^{-0.27}$ and a high-intensity dependence of $I_1^{-1.5}$, further indicating a speeding-up of exciton thermalization at high intensities.

In our FWM experiment, the photoinduced absorption of excitons would result in a decrease of the signal and cannot be distinguished from the dominant absorption bleaching. However, in line with the discussion in the previous section, the presence of photoinduced absorption is supported by the dip observed at negative delays. Its presence at high excitation intensities is due to destructive interference between the leftover signal due to previous pulses and the FWM generated by the P_1 - P_2 - P_3 pulse sequence with P_3 in time overlap with the reference pulse. The inset of Figure 8(b) shows the dynamics of the FWM field phase for three excitation intensities corresponding to N_{ex} equal to 0.02, 0.7, and 2.9, respectively. At low intensity, the phase at negative and positive delays is similar, indicating that the signal measured at negative delays is due to absorption bleaching induced by the leftover exciton density generated by previous pulses. With increasing intensity, the phase difference between the signal at negative and positive delays increases and reaches $\sim 0.75\pi$ for $N_{\text{ex}} = 2.9$. This suggests that the origin of the signal at negative delays is different from absorption bleaching.

Thermal effects can produce a phase shift of the FWM signal of $\pi/2$, while photoinduced absorption should give a phase shift of π . Since the measured phase shift exceeds 0.5π , induced absorption is a significant process.⁵² The continuous change of the phase difference with intensity indicates that the signals of the induced absorption and the absorption bleaching are not π out of phase. While the resonant absorption bleaching will not be accompanied by a resonant phase component, the photoinduced absorption can, provided that it is not spectrally centered at the excitation wavelengths. This will be the case, e.g., when photoinduced absorption involves transitions to higher energy conduction or valence band states of the Qdots.

The observation that photoinduced absorption starts to dominate the FWM signal at negative delays with increasing light intensity may reflect the presence of charges in the Qdots, related to the occurrence of Auger events at high exciton densities. As a result of an Auger process, one of the carriers can be trapped by a defect state at high energy or leave the Qdot to be trapped in its vicinity. In this situation, the cross section of the absorption bleaching broadens as compared to that of resonantly excited Qdots in their ground state. On the other hand, the cross section of the photoinduced absorption has most likely a broad spectrum. Hence, it will not be significantly affected by the redistribution of the carriers.

IV. DISCUSSION

The measurements presented here demonstrate that resonantly excited PbS Qdots have a large nonlinear refractive index, with a figure of merit that exceeds one. This optical nonlinearity is related to the creation of excitons and to photoinduced absorption—possibly intraband absorption—in already excited Qdots. Relaxation and recombination of excitons lead to a complex nonlinear dynamics, with distinct time constants of the order of 100 ps and 1 ns next to the single exciton lifetime of about 1 μs . Furthermore, like PbSe Qdots, the n_2 spectrum of PbS Qdots shows a bell shape, which contrasts with the dispersive, antiresonance behavior predicted for the two-level system.⁵¹ This can mean that the optical nonlinearity is dominated by photoinduced absorption,

which is typically a spectrally broad process that does not result in the dispersive n_2 of the two-level system. Alternatively, the n_2 spectrum can also have the observed bell shape if biexciton absorption is the dominant process. Although biexciton absorption should also lead to an antiresonance in n_2 , its resonance frequency is slightly red shifted due to the biexciton binding energy.⁴⁷ Hence, biexciton absorption will always give a negative contribution to n_2 , regardless of the wavelength used.

The Z-scan measurements do not allow for a decomposition of n_2 into the separate contribution from exciton creation and photoinduced absorption. Nevertheless, a number of arguments suggest that the contribution from photoinduced absorption is considerable. First, opposite to the nonlinear absorption, the nonlinear refraction does not show a tendency to saturate with increasing light intensity. This saturation would be expected if only exciton creation contributed to n_2 . Second, the intensity dependence of the absorption could only be modeled if we include photoinduced absorption from the exciton ground state to an excited exciton state. Finally, the FWM experiments, revealed that photoinduced absorption dominates absorption bleaching of the probing pulse at negative time delays.

V. CONCLUSIONS

We have studied the nonlinear properties of PbS Qdot suspensions as a function of wavelength, optical intensity and Qdot volume fraction using the Z-scan technique with picosecond pulses. Knowing the characteristic temperature profile buildup time t_c , we modulated the laser repetition rate and excluded thermal lensing to directly measure the electronic contribution to n_2 . The nonlinear refractive index is independent from the intensity and follows the Qdot absorption spectrum. The FOM is larger than one for the PbS Qdots and is comparable with PbSe Qdots and lead chalcogenide glasses. It is argued that the creation of excitons and the resulting photoinduced absorption in the PbS Qdots lie at the origin of the observed n_2 and β . Using transient four wave mixing with 150-fs pulses we proved that at low excitation intensities the dynamics is dominated by single-exciton thermalization (ns) and recombination (μs). At higher intensities, the FWM signal results in a 100-ps response. This shows that colloidal PbS Qdots are efficient and fast nonlinear materials. In combination with the facile integration of PbS Qdots with photonic devices using wet deposition techniques and the easy tuning of the Qdot linear and nonlinear properties,⁵³ this opens pathways for all-optical signal processing on photonic platforms.

ACKNOWLEDGMENTS

We acknowledge the Institute for the Promotion of Innovation through Science and Technology in Flanders (IWT-Vlaanderen) for a scholarship (A.O.). I.M. is a postdoctoral researcher with the FWO Vlaanderen. This project was also supported by the Belgian Science Policy Office (IAP P6/10), the EU Seventh Framework Program (EU-FP7 ITN Herodot) and the FWO-Vlaanderen (G.0144.08). F.M. acknowledges funding from the European Community's Seventh Framework

Programm [FP7/2007-2013] under grant agreement [PIEF-GA-2008-220901].

APPENDIX A: DETERMINATION OF N_{ex}

The number of excitations or absorbed photons per unit of volume created per pulse, N_{ph} , equals

$$N_{\text{ph}} = \frac{E_{\text{abs}}}{E_{\text{gap}}L} \quad (\text{A1})$$

with L the sample length and E_{abs} the absorbed energy per unit of area following an excitation with a pulse. For $\alpha L \ll 1$, we find for E_{abs} ,

$$E_{\text{abs}} = \frac{P}{\nu\pi w_0^2} \alpha(E_{\text{gap}})L \quad (\text{A2})$$

with $\alpha(E_{\text{gap}}) \approx \alpha_0(E_{\text{gap}})$, with $\alpha_0(E_{\text{gap}})$ the linear absorption coefficient at the band gap energy. This approximation is valid in our case as α maximally decrease with 20% over the measured intensity range (see Fig. 7). P_{avg} is the average laser power and is related to I_0 through expression (2). The number of excitations per pulse created per Qdot N_{ex} is

$$N_{\text{ex}} = \frac{N_{\text{ph}}}{c_{\text{ex}}N_A} \quad (\text{A3})$$

with c_{ex} the concentration of Qdots excited with the laser beam. c_{ex} is determined as

$$c_{\text{ex}} = c_{\text{tot}} \int c(E)S(E)dE, \quad (\text{A4})$$

where c_{tot} is the total Qdot concentration and $c(E)dE$ represents the fraction of Qdots with a band gap in the energy range $E, E + dE$. $S(E)$ represents the probability that a Qdot with band gap E gets excited with the corresponding laser beam. $c(E)$ and $S(E)$ are given by

$$c(E) = \frac{1}{\sqrt{2\pi}\sigma_{\text{inh}}} e^{-\frac{(E-E_{\text{gap}})^2}{2\sigma_{\text{inh}}^2}}, \quad (\text{A5})$$

$$S(E) = e^{-\frac{(E-E_l)^2}{2(\sigma_l^2 + \sigma_{\text{hom}}^2)}}, \quad (\text{A6})$$

with E_l central energy of the Gaussian laser beam and $\sigma_l = \frac{\Delta E_l}{2\sqrt{2\ln(2)}}$, with ΔE_l , the FWHM of the laser beam. Similarly, $\sigma_l = \frac{\Delta E_{\text{hom}}}{2\sqrt{2\ln(2)}}$ and $\sigma_{\text{inh}} = \frac{\Delta E_{\text{inh}}}{2\sqrt{2\ln(2)}}$ with ΔE_{hom} and ΔE_{inh} , respectively, the homogenous and inhomogenous linewidth of the Qdots.

As the size dispersion is very small (5%), one can assume the inhomogenous linewidth to be constant for all Qdots.⁵⁰ Evaluation of expression (A4) for c_{ex} yields

$$c_{\text{ex}} = c_{\text{tot}} \frac{e^{-\frac{(E_{\text{gap}}-E_l)^2}{2(\sigma_{\text{inh}}^2 + \sigma_l^2 + \sigma_{\text{hom}}^2)}} \sqrt{\sigma_l^2 + \sigma_{\text{hom}}^2}}{\sqrt{\sigma_{\text{inh}}^2 + \sigma_l^2 + \sigma_{\text{hom}}^2}}. \quad (\text{A7})$$

This leads to a final expression for N_{ex} presuming that we excite with a central laser energy in resonance with the band-gap energy ($E_l = E_{\text{gap}}$):

$$N_{\text{ex}} = \frac{\sqrt{\pi}\tau_p I_0 \alpha_0(E_{\text{gap}}) \sqrt{\Delta E_{\text{inh}}^2 + \Delta E_l^2 + \Delta E_{\text{hom}}^2}}{2E_{\text{gap}} c_{\text{tot}} N_A \sqrt{\Delta E_l^2 + \Delta E_{\text{hom}}^2}}. \quad (\text{A8})$$

The factor $\sqrt{\Delta E_{\text{inh}}^2 + \Delta E_l^2 + \Delta E_{\text{hom}}^2}$ represents the total linewidth of the Qdots.

APPENDIX B: DETERMINATION OF $\alpha(I_0)$

We define c_i as the fraction of total Qdots which contain i excitons. The number i can maximally reach eight due to the eightfold degeneracy of the HOMO and LUMO levels in the PbS Qdots. Within the duration of each incoming pulse, the occupancy of the different c_i changes with time due to the absorption and stimulated emission of photons. This yields

$$\begin{aligned} \frac{dc_0}{dt} &= -k_{0,\text{abs}}c_0 + k_{1,\text{em}}c_1, \\ \frac{dc_1}{dt} &= k_{0,\text{abs}}c_0 - k_{1,\text{abs}}c_1 - k_{1,\text{em}}c_1 + k_{2,\text{em}}c_2, \\ \frac{dc_2}{dt} &= k_{1,\text{abs}}c_1 - k_{2,\text{abs}}c_2 - k_{2,\text{em}}c_2 + k_{3,\text{em}}c_3, \\ &\dots \\ \frac{dc_7}{dt} &= k_{6,\text{abs}}c_6 - k_{7,\text{abs}}c_7 - k_{7,\text{em}}c_7 + k_{8,\text{em}}c_8, \\ \frac{dc_8}{dt} &= k_{7,\text{abs}}c_7 - k_{8,\text{em}}c_8. \end{aligned} \quad (\text{B1})$$

Here, $k_{i,\text{abs}}$ is the rate of absorption of a state i , which is given by $\frac{i-8}{8}k_{0,\text{abs}}$. $k_{0,\text{abs}}$ is the rate of absorption by an unexcited state Qdot, which corresponds to $\frac{\epsilon \ln(10)I_0}{N_A E_{\text{gap}}}$. With ϵ the molar extinction coefficient determined as $\frac{2\sqrt{2\ln(2)}}{\sqrt{2\pi}} \frac{\epsilon_{\text{int}}}{\Delta E_{\text{hom}}}$. ϵ_{int} is the integrated molar extinction value, which is given by $15.3 \frac{\text{meV}}{\mu\text{Mcm}}$.⁵⁴ $k_{i,\text{em}}$ is the stimulated emitting rate from a state i to a state $(i-1)$ and is given by $\frac{i}{8}k_{0,\text{abs}}$.

Between the pulses we assume $c_i \rightarrow 0$, i.e., that the relaxation of the states c_i , $i = 2, \dots, 8$ is much faster than the laser repetition period of 100 ns. This means that the remaining relaxation contribution is due to 1 μs radiative recombination⁵⁴ of state c_1 . By implementing this procedure numerically, one can calculate for a given ΔE_{hom} and I_0 the average number of excitons in the Qdots through

$$\langle \gamma(t) \rangle = \left\langle \sum i c_i(t) \right\rangle. \quad (\text{B2})$$

The corresponding absorption coefficient is calculated using Eq. (10).

*abdoulghafar.omari@ugent.be

†zeeger.hens@ugent.be

¹G. Priem, I. Notebaert, B. Maes, P. Bienstman, G. Morthier, and R. Baets, *IEEE J. Sel. Top. Quantum Electron.* **10**, 1070 (2004).

²C. Koos, L. Jacome, C. Poulton, J. Leuthold, and W. Freude, *Opt. Express* **15** 5976 (2007).

³M. A. Petruska, A. V. Malko, P. M. Voyles, and V. I. Klimov, *Adv. Mater.* **15**, 610 (2003).

- ⁴B. H. Cumpston, S. P. Ananthavel, S. Barlow, D. L. Dyer, J. E. Ehrlich, L. L. Erskine, A. A. Heikal, S. M. Kuebler, I. Y. S. Lee, D. McCord-Maughon, J. Q. Qin, H. Rockel, M. Rumi, X. L. Wu, S. R. Marder, and J. W. Perry, *Nature (London)* **398**, 51 (1999).
- ⁵S. Kawata, H. B. Sun, T. Tanaka, and K. Takada, *Nature (London)* **412**, 697 (2001).
- ⁶J. Serbin, A. Egbert, A. Ostendorf, B. N. Chichkov, R. Houbertz, G. Domann, J. Schulz, C. Cronauer, L. Frohlich, and M. Popall, *Opt. Lett.* **28**, 301 (2003).
- ⁷A. Villeneuve, C. C. Yang, G. I. Stegeman, C. H. Lin, and H. H. Lin, *Appl. Phys. Lett.* **62**, 2465 (1993).
- ⁸M. Dinu, F. Quochi, and H. Garcia, *Appl. Phys. Lett.* **82**, 2954 (2003).
- ⁹G. Lenz, J. Zimmermann, T. Katsufuji, M. E. Lines, H. Y. Hwang, S. Splter, R. E. Slusher, S. W. Cheong, J. S. Sanghera, and I. D. Aggarwal, *Opt. Lett.* **25**, 254 (2000).
- ¹⁰J. M. Harbold, F. O. Ilday, F. W. Wise, J. S. Sanghera, V. Q. Nguyen, L. B. Shaw, and I. D. Aggarwal, *Opt. Lett.* **27**, 119 (2002).
- ¹¹T. G. Juliet, S. Marin, P. I. Erich, N. F. Vladimir, A. K. Wesley, and S. Max, *J. Appl. Phys.* **96**, 6931 (2004).
- ¹²B. Esembeson, M. L. Scimeca, T. Michinobu, F. Diederich, and I. Biaggio, *Adv. Mater.* **20**, 4584 (2008).
- ¹³T. Vallaitis, S. Bogatscher, L. Alloatti, P. Dumon, R. Baets, M. L. Scimeca, I. Biaggio, F. Diederich, C. Koos, W. Freude, and J. Leuthold, *Opt. Express* **17**, 17357 (2009).
- ¹⁴S. Coe-Sullivan, *Nat. Photonics* **3**, 315 (2009).
- ¹⁵C. Koos, P. Vorreau, T. Vallaitis, P. Dumon, W. Bogaerts, R. Baets, B. Esembeson, I. Biaggio, T. Michinobu, F. Diederich, W. Freude, and J. Leuthold, *Nat. Photonics* **3**, 216219 (2009).
- ¹⁶J. S. Steckel, P. Snee, S. Coe-Sullivan, J. P. Zimmer, J. E. Halpert, P. Anikeeva, L.-A. Kim, V. Bulovic, and M. G. Bawendi, *Angew. Chem.-Int. Edit.* **45**, 5796 (2006).
- ¹⁷A. L. Rogach, N. Gaponik, J. M. Lupton, C. Bertoni, D. E. Gallardo, S. Dunn, N. Li Pira, M. Paderi, P. Repetto, S. G. Romanov, C. O'Dwyer, C. M. Sotomayor Torres, and A. Eychmüller, *Angew. Chem.-Int. Edit.* **47**, 6538 (2008).
- ¹⁸A. V. Malko, A. A. Mikhailovsky, M. A. Petruska, J. A. Hollingsworth, H. Htoon, M. G. Bawendi, and V. I. Klimov, *Appl. Phys. Lett.* **81**, 1303 (2002).
- ¹⁹R. D. Schaller, M. A. Petruska, and V. I. Klimov, *J. Phys. Chem. B* **107**, 13765 (2003).
- ²⁰V. I. Klimov, S. A. Ivanov, J. Nanda, M. Achermann, I. Bezel, J. A. McGuire, and A. Piryatinski, *Nature (London)* **447**, 441 (2007).
- ²¹S. A. McDonald, G. Konstantatos, S. G. Zhang, P. W. Cyr, E. J. D. Klem, L. Levina, and E. H. Sargent, *Nat. Mater.* **4**, 138 (2005).
- ²²T. Rauch, M. Boberl, S. F. Tedde, J. Furst, M. V. Kovalenko, G. N. Hesser, U. Lemmer, W. Heiss, and O. Hayden, *Nat. Photonics* **3**, 332 (2009).
- ²³I. Moreels, Z. Hens, P. Kockaert, J. Loicq, and D. Van Thourhout, *Appl. Phys. Lett.* **89**, 193106 (2006).
- ²⁴A. A. Lagatsky, C. T. A. Brown, and W. Sibbett, *Optics Express* **12**, 3928 (2004).
- ²⁵A. A. Lagatsky, A. M. Malyarevich, V. G. Savitski, M. S. Gaponenko, K. V. Yumashev, A. A. Zhilin, C. T. A. Brown, and W. Sibbett, *IEEE Photonics Technol. Lett.* **18**, 259 (2006).
- ²⁶L. A. Padilha, G. Nootz, P. D. Olszak, S. Webster, D. J. Hagan, E. W. Van Stryland, L. Levina, V. Sukhovatkin, L. Brzozowski, and E. H. Sargent, *Nano Lett.* **11**, 1227 (2011).
- ²⁷G. Nootz, L. A. Padilha, P. D. Olszak, S. Webster, D. J. Hagan, E. W. Van Stryland, L. Levina, V. Sukhovatkin, L. Brzozowski, and E. H. Sargent, *Nano Lett.* **10**, 3577 (2010).
- ²⁸H. P. Li, B. Liu, C. H. Kam, Y. L. Lam, W. X. Que, L. M. Gan, C. H. Chew, and G. Q. Xu, *Opt. Mater.* **14**, 321 (2000).
- ²⁹A. M. Malyarevich, M. S. Gaponenko, K. V. Yumashev, A. A. Lagatsky, W. Sibbett, A. A. Zhilin, and A. A. Lipovskii, *J. Appl. Phys.* **100**, 023108 (2006).
- ³⁰D. Li, C. Liang, Y. Liu, and S. Qian, *J. Lumin.* **122-123**, 549 (2007).
- ³¹D. J. Asunskis, I. L. Bolotin, and L. Hanley, *J. Phys. Chem. C* **112**, 9555 (2008).
- ³²D. J. Asunskis, I. L. Bolotin, J. E. Haley, A. Urbas, and L. Hanley, *J. Phys. Chem. C* **113**, 19824 (2009).
- ³³I. L. Bolotin, D. J. Asunskis, A. M. Jawaid, Y. Liu, P. T. Snee, and L. Hanley, *J. Phys. Chem. C* **114**, 16257 (2010).
- ³⁴F. Yoshino, A. Major, L. Brzozowski, L. Levina, V. Sukhovatkin, and E. H. Sargent, *Proceedings of the Society of Photo-Optical Instrumentation Engineers (SPIE)* **5361**, 142 (2004).
- ³⁵F. Yoshino, A. A. Major, L. Levina, and E. H. Sargent, International Quantum Electronics Conference (IQEC) (IEEE Cat. No. 04CH37598) (2004).
- ³⁶L. Brzozowski, E. H. Sargent, and M. A. Hines, CLEO/Pacific Rim 2003. The 5th Pacific Rim Conference on Lasers and Electro-Optics (IEEE Cat. No. 03TH8671) **2**, 461 (2003).
- ³⁷V. G. Savitski, A. M. Malyarevich, M. I. Demchuk, K. V. Yumashev, H. Raaben, and A. A. Zhilin, *J. Opt. Soc. Am. B* **22**, 1660 (2005).
- ³⁸D. Milam, *Appl. Opt.* **37**, 546 (1998).
- ³⁹M. Sheikbaha, A. A. Said, T. H. Wei, D. J. Hagan, and E. W. Vanstryland, *IEEE J. Quantum Electron.* **26**, 760 (1990).
- ⁴⁰M. Falconieri, *J. Opt. A* **1**, 662 (1999).
- ⁴¹F. Masia, I. Moreels, Z. Hens, W. Langbein, and P. Borri, *Phys. Rev. B* **82**, 155302 (2010).
- ⁴²This leads to a 1-MHz modulation of the carrier density.
- ⁴³I. Moreels, Y. Justo, B. De Geyter, K. Haustraete, J. C. Martins, and Z. Hens, *Acs Nano* **5**, 2004 (2011).
- ⁴⁴S. Valkai, J. Liszi, and I. Szalai, *J. Chem. Thermodyn.* **30**, 825 (1998).
- ⁴⁵E.-K. Hassan, *Rev. Sci. Instrum.* **69**, 1243 (1998).
- ⁴⁶D. R. Lide, *CRC Handbook of Chemistry and Physics*, 82nd ed. (CRC press, Boca Raton, Florida, USA, 2001).
- ⁴⁷Y. Gao, E. Talgorn, M. Aerts, M. T. Trinh, J. M. Schins, A. J. Houtepen, and L. D. a. Siebbeles, *Nano Lett.* **11**, 5471 (2011).
- ⁴⁸E. Istrate, S. Hoogland, V. Sukhovatkin, L. Levina, S. Myrskog, P. W. E. Smith, and E. H. Sargent, *J. Phys. Chem. B* **112**, 2757 (2008).
- ⁴⁹G. Nootz, L. Padilha, L. A. Levina, V. Sukhovatkin, S. Webster, L. A. Brzozowski, E. H. Sargent, D. J. Hagan, and E. W. Van Stryland, *Phys. Rev. B* **83**, 155302 (2011).
- ⁵⁰F. Masia, W. Langbein, I. Moreels, Z. Hens, and P. Borri, *Phys. Rev. B* **83**, 201309 (2011).
- ⁵¹R. W. Boyd, *Nonlinear Optics*, 2nd ed. (Academic Press, San Diego, USA, 2003).
- ⁵²The effect of heating can be neglected. Considering the beam size and the thermal diffusion coefficient of the polystyrene,⁵⁵ we estimate for the FWM experiment, a characteristic heating build up time 2×10^3 time faster than in the Z-scan experiment, with an on state of the excitation 4×10^3 times shorter. As a consequence,

the heating effects are attenuated by a factor of two in the FWM experiment with respect to the *Z*-scan measurements, where it is negligible.

⁵³I. Moreels, B. De Geyter, D. Van Thourhout, and Z. Hens, *J. Opt. Soc. Am. B* **26**, 1243 (2009).

⁵⁴I. Moreels, K. Lambert, D. Smeets, D. De Muynck, T. Nollet, J. C. Martins, F. Vanhaecke, A. Vantomme, C. Delerue, G. Allan, and Z. Hens, *Acs Nano* **3**, 3023 (2009).

⁵⁵M. Hattori, *Kolloid-Zeitschrift und Zeitschrift für Polymere* **202**, 11 (1964).